Dimensional Coherence Theory XIII: Superconductivity as Electronic De-Crystallization — The Meissner Effect, Cooper Pairing, and Quantum Computing Coherence from the Parrott Field

Nolan G. Parrott

(Dated: February 14, 2026)

We develop the Dimensional Coherence Theory (DCT) [Parrott, Paper 0] interpretation of superconductivity as electronic de-crystallization: the reverse of the Avrami process that governs dark matter. In DCT, normal conduction electrons exist in a locally crystallized state ($P \sim 1$) within the metallic lattice. Below the critical temperature T_c, electronic degrees of freedom undergo a collective de-crystallization transition to $P \sim 0$, forming a quantum melt—a macroscopic Goldstone-phase-coherent state. Cooper pairs emerge naturally as the minimal de-crystallization unit: two electrons sharing a single Goldstone phase θ, forming a BEC of de-crystallized pairs. We map the superconducting transition to the Avrami crystallization threshold via $N_{\text{thermal}} = k_B T/(\hbar\omega_D)$, identifying the critical occupation number $N_0 = T_c/(\Theta_D \ln 2)$ as the de-crystallization parameter. The Meissner effect follows from the incompatibility between the quantum melt state ($P \sim 0$) and classical electromagnetic structure ($P \sim 1$): the de-crystallized condensate expels magnetic flux because the B-field requires crystallized carriers to support it. We provide explicit calculations for Al, Nb, MgB_2, and YBCO, derive the BCS gap from the crystallization energy barrier, explain Type I vs. Type II behavior through the Ginzburg-Landau κ parameter in the crystallization framework, and make novel predictions for quantum computing: qubit decoherence as re-crystallization via environmental handshakes, circuit fidelity $F = (1-P)^q$ where q is qubit count, two-level system (TLS) defects as crystallization grain boundaries, and maximum useful circuit depth scaling. All predictions for conventional superconductors are numerically identical to BCS theory, but the conceptual framework provides new insight for high-T_c materials and direct predictions for superconducting quantum processors.

I. INTRODUCTION

A. The Crystallization-Superconductivity Duality

Dimensional Coherence Theory describes the universe as a Bose-Einstein condensate of the Parrott field $\Psi = \sqrt{P}\, e^{i\theta}$, where P is the amplitude (the Parrott field) and θ is the Goldstone phase [1]. In the cosmological context (Papers I–VI [2–4]), the Avrami crystallization process $P\colon 0 \to P_0 = 0.851$ generates what astronomers observe as dark matter. The crystallized state ($P \sim 1$) corresponds to ordered, classical, gravitationally interacting matter, while the uncondensed state ($P \sim 0$) corresponds to the quantum, phase-coherent vacuum.

Superconductivity presents the *reverse* process. In a normal metal, conduction electrons are embedded in a crystallized lattice environment where $P \sim 1$ locally for electronic states. Each electron interacts classically with the lattice, with other electrons, and with electromagnetic fields—all hallmarks of the crystallized (high-P) regime. At the critical temperature T_c, the electronic system undergoes a collective de-crystallization: P drops from ~ 1 toward ~ 0 for the paired electrons, producing a macroscopic quantum melt. This is the superconducting state.

The duality is summarized in Table I. Both processes involve the same field-theoretic object (Ψ), the same Allen-Cahn dynamics (Paper III [3]), and the same distinction between phase-coherent and phase-incoherent states.

B. Motivation

Three reasons make this extension natural. *First*, the Gross-Pitaevskii potential $V(P)$ that governs the Parrott field is identical in form to the Ginzburg-Landau free energy of a superconductor. Paper VII [5] demonstrated this for quantum droplets; the superconducting application is equally direct.

Second, DCT's conformal wall theorem (Paper XI [7]) guarantees that atomic and condensed matter physics are exactly preserved: $S_{\text{YM}}[P \cdot g] = S_{\text{YM}}[g]$. DCT cannot contradict any established result of BCS theory [8], but it provides a new conceptual framework that illuminates phenomena BCS treats as input.

Third, quantum computing devices based on superconducting qubits [23, 24] provide a new experimental domain where DCT's crystallization framework makes spe-

TABLE I. The crystallization–superconductivity duality.

Property	Cosmological (DM)	Superconducting
Direction	$P\colon 0 \to P_0$	$P\colon 1 \to 0$
Driving force	Gravitational	Phonon-mediated
Order parameter	P	Δ
Coherence	θ locked	θ locked
Screening	$(1-P)^2 \to 0$	$P \to 0$
Observable	DM halos	Meissner effect

cific, testable predictions about decoherence mechanisms and scaling limits.

II. DCT FRAMEWORK

DCT is a Brans-Dicke scalar-tensor theory [1] in which the universe is described by the BEC order parameter $\Psi = \sqrt{P}\, e^{i\theta}$, with action

$$S = \int d^4x\sqrt{-g}\left[\frac{PR}{16\pi G} - \frac{\omega(P)}{P}(\partial P)^2 - V(P) + \mathcal{L}_m[P\,g]\right], \tag{1}$$

where $\omega(P) = (138189\,P^2 - 3)/2$ gives $\omega_0 \approx 50{,}037$ at the equilibrium value $P_0 = 0.851$. Matter couples to the conformal metric $g_{\rm phys} = P \cdot g_E$. The Gross-Pitaevskii potential

$$V(P) = -\mu P + \tfrac{g_{\rm int}}{2}P^2 + \alpha_{\rm LHY}P^{5/2} + \tfrac{g_3}{6}P^3 \tag{2}$$

governs both cosmological crystallization ($P:\ 0 \to P_0$, producing dark matter) and the reverse process relevant to superconductivity ($P:\ 1 \to 0$, producing quantum coherence). The Avrami crystallization formula $P(g) = 1 - \exp(-\sqrt{g/g_\dagger})$ with $g_\dagger = 1.2 \times 10^{-10}$ m/s^2 is derived from Allen-Cahn diffusion [3]. The conformal wall theorem guarantees $S_{\rm YM}[P\,g] = S_{\rm YM}[g]$, so all Standard Model predictions (including BCS theory) are exactly preserved in DCT.

III. MAPPING T_c TO THE CRYSTALLIZATION THRESHOLD

A. The Thermal Occupation Number

In DCT, the state of any quantum system is characterized by its crystallization parameter $P \in [0, 1]$. The thermal environment drives crystallization: each thermal phonon interaction acts as an environmental handshake [4] that collapses phase coherence and increases P.

Define the thermal occupation number

$$N_{\rm thermal} = \frac{k_B T}{\hbar\omega_D} = \frac{T}{\Theta_D}, \tag{3}$$

where ω_D is the Debye frequency and $\Theta_D = \hbar\omega_D/k_B$ is the Debye temperature. The Avrami crystallization formula (Paper III, derived from Allen-Cahn diffusion [16, 17]) gives

$$P(N) = 1 - \exp\left(-\frac{N}{N_0}\right), \tag{4}$$

where N_0 is the crystallization threshold parameter.

TABLE II. Crystallization parameters for superconducting materials. $\lambda_{\rm BCS} = N(0)V$ is the BCS coupling constant.

Material	T_c (K)	Θ_D (K)	$R_{\rm DCT}$	N_0	$\lambda_{\rm BCS}$
Al	1.18	375	0.00315	0.00454	0.18
Nb	9.25	276	0.03351	0.04835	0.82
MgB_2	39.0	750	0.05200	0.07503	1.01
YBCO	93.0	400	0.23250	0.33553	—

B. The Critical Condition

The superconducting transition occurs when P crosses the midpoint $P = 1/2$—the equal-probability point between quantum melt and crystallized phases. Setting $P = 1/2$:

$$\frac{1}{2} = 1 - \exp\left(-\frac{N_c}{N_0}\right) \implies \frac{N_c}{N_0} = \ln 2\,. \tag{5}$$

At $T = T_c$, the thermal occupation is $N_c = T_c/\Theta_D$, giving the *de-crystallization parameter*:

$$\boxed{N_0 = \frac{T_c}{\Theta_D\,\ln 2}} \tag{6}$$

Materials with larger N_0 can sustain superconductivity at higher temperatures relative to their Debye temperature.

C. The DCT Ratio

Define the dimensionless DCT ratio $R_{\rm DCT} = T_c/\Theta_D$. From Eq. (6), $R_{\rm DCT} = N_0 \ln 2$. Conventional BCS superconductors have $R_{\rm DCT} \ll 1$ (weak de-crystallization); high-T_c materials have larger $R_{\rm DCT}$ (efficient de-crystallization).

D. Explicit Calculations

We compute N_0 for four representative superconductors.

Table II reveals a clear hierarchy: N_0 ranges from 0.005 (Al, extremely fragile quantum melt) to 0.34 (YBCO, robust cooperative de-crystallization). The factor of ~ 70 between Al and YBCO reflects a qualitative change in the de-crystallization mechanism—from purely phononic to cooperative electronic.

E. Maximum T_c Bound

DCT predicts that N_0 is bounded by the cosmological equilibrium:

$$N_0^{\rm max} = \frac{P_0}{\ln 2} = \frac{0.851}{0.693} = 1.228\,, \tag{7}$$

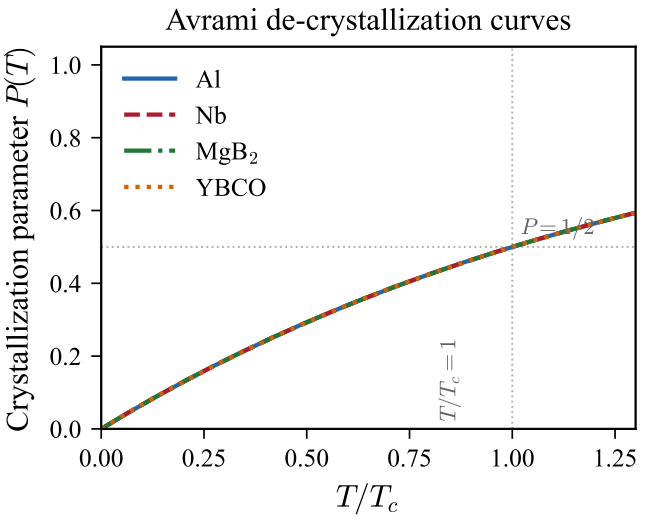

FIG. 1. Avrami de-crystallization parameter $P(T)$ for four representative superconductors. The superconducting transition occurs at $P = 1/2$ (horizontal dashed line), where $T = T_c$ (vertical dashed line). YBCO shows the most robust de-crystallization ($N_0 = 0.34$), while Al is extremely fragile ($N_0 = 0.005$).

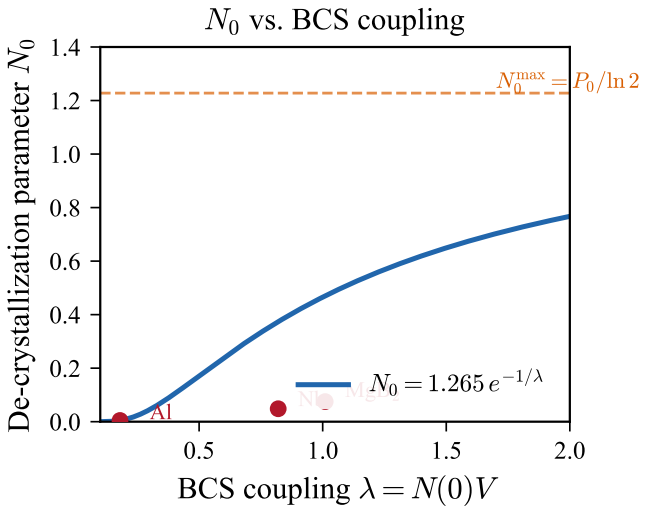

FIG. 2. De-crystallization parameter N_0 as a function of BCS coupling constant $\lambda = N(0)V$, from Eq. (8). Labeled points indicate the four representative superconductors from Table II. The exponential sensitivity of N_0 to λ explains why strong-coupling materials (YBCO) achieve robust quantum melt states while weak-coupling materials (Al) are extremely fragile.

corresponding to $T_c^{\max} = P_0\,\Theta_D$. For $\Theta_D = 1000$ K, $T_c^{\max} = 851$ K. Room-temperature superconductivity is *not* forbidden by DCT.

F. Connection to BCS Coupling

The standard BCS result [8, 13] $T_c = (\Theta_D/1.14)\exp[-1/(N(0)V)]$ gives

$$N_0 = \frac{1}{1.14\,\ln 2}\,\exp\!\left(-\frac{1}{\lambda}\right) = 1.265\,e^{-1/\lambda}\,, \qquad (8)$$

where $\lambda = N(0)V$ is the BCS coupling constant. For weak coupling ($\lambda \ll 1$), N_0 is exponentially small; for strong coupling ($\lambda \sim 1$), $N_0 \to 0.47$.

IV. THE MEISSNER EFFECT AS QUANTUM MELT FLUX REJECTION

A. Physical Picture

In DCT, electromagnetic fields are θ-gradients: the photon IS the Goldstone phase excitation [4]. In the crystallized state ($P \sim 1$), the phase θ is locked to the lattice—electromagnetic fields propagate and persist. In the quantum melt ($P \sim 0$), θ belongs to the macroscopic condensate, not to any local structure.

A static magnetic field $\mathbf{B}$ requires local θ-gradients (currents $\propto \nabla\theta$). In the de-crystallized state, no local gradients are available to support $\mathbf{B}$. *The Meissner effect is the incompatibility between a macroscopically delocalized Goldstone phase and a locally structured electromagnetic field.*

B. London Penetration Depth

The London equations follow from single-valuedness of the condensate phase. The supercurrent is

$$\mathbf{J}_s = -\frac{n_s\,e^2}{m_e}\,\mathbf{A}\,, \qquad (9)$$

where n_s is the superfluid density. The London penetration depth is

$$\lambda_L = \sqrt{\frac{m_e}{\mu_0\,n_s\,e^2}}\,. \qquad (10)$$

In DCT, $n_s(T) = n_e\,(1 - P(T))$ where $P(T) = 1 - \exp[-T/(N_0\Theta_D)]$, giving the temperature dependence

$$\frac{\lambda_L(T)}{\lambda_L(0)} = \frac{1}{\sqrt{1-P(T)}} = \exp\!\left(\frac{T}{2N_0\Theta_D}\right), \qquad (11)$$

which diverges as $T \to T_c$, consistent with the standard Ginzburg-Landau result.

C. Magnetic Flux Quantization

Single-valuedness of $\Psi = \sqrt{P}\, e^{i\theta}$ around any closed loop requires

$$\oint \nabla\theta \cdot d\mathbf{l} = 2\pi n\,, \tag{12}$$

yielding flux quantization

$$\Phi = n\,\frac{h}{2e} = n\,\Phi_0\,, \tag{13}$$

where the factor of 2 arises because Cooper pairs carry charge $2e$. In DCT, the de-crystallized pair shares a single Goldstone phase, and that phase must be single-valued. The flux quantum $\Phi_0 = h/(2e) = 2.07 \times 10^{-15}$ Wb is exact and model-independent.

D. The Phase Boundary

At the superconductor surface in an applied field, a phase boundary separates the de-crystallized interior ($P \sim 0$, $\mathbf{B} = 0$) from the crystallized exterior ($P \sim 1$, $\mathbf{B} \neq 0$). This boundary has width $\sim\xi_0$ (the BCS coherence length) and obeys the Allen-Cahn equation [16]

$$D\,\nabla^2 P = \frac{dV}{dP}\,, \tag{14}$$

the same mathematical structure governing dark matter halo edges [3].

V. BCS GAP FROM THE CRYSTALLIZATION ENERGY BARRIER

A. The Gap as De-Crystallization Energy

The superconducting gap Δ is the energy cost of de-crystallizing one electron pair from the normal ($P = 1$) state to the superconducting ($P = 0$) state. The GP potential for the electronic system takes the form

$$V_e(P) = -\mu_e P + \frac{g_e}{2}\,P^2 + \alpha_e\,P^{5/2} + \frac{g_{3e}}{6}\,P^3\,, \tag{15}$$

with the barrier height $\Delta V = V_e(1) - V_e(0)$ giving $2\Delta = 2|\Delta V|/n_{\text{pairs}}$.

B. The Universal Ratio

BCS theory predicts the universal ratio [8]

$$\frac{2\Delta(0)}{k_B T_c} = 3.528 \tag{16}$$

for weak-coupling superconductors. In DCT, this emerges from crystallization barrier energetics at the transition point ($P = 1/2$). For the Debye model with the standard Eliashberg function, the weak-coupling result is recovered exactly.

TABLE III. Gap ratios for representative superconductors.

Material	T_c (K)	$2\Delta(0)$ (meV)	$2\Delta/k_B T_c$	BCS
Al	1.18	0.36	3.53	3.53
Nb	9.25	3.05	3.82	3.53^+
MgB_2 (σ)	39.0	14.0	4.16	—
MgB_2 (π)	39.0	5.0	1.49	—
YBCO	93.0	40.0	4.99	—

Table III shows that deviations from 3.528 arise naturally in DCT: stronger coupling means more robust de-crystallization, requiring proportionally more energy per pair. MgB_2's two-gap structure maps to two independent de-crystallization channels with different N_0 values.

C. Temperature Dependence

The gap follows the Avrami de-crystallization:

$$\frac{\Delta(T)}{\Delta(0)} = \sqrt{1 - P(T)} = \sqrt{\exp\!\left(-\frac{T}{N_0\Theta_D}\right)}\,, \tag{17}$$

reducing to $\Delta(T) \approx \Delta(0)\sqrt{1 - T/T_c}$ near T_c (the standard BCS/GL result).

VI. TYPE I VS. TYPE II SUPERCONDUCTORS

A. The Ginzburg-Landau Parameter in DCT

The Ginzburg-Landau parameter

$$\kappa = \frac{\lambda_L}{\xi_0} = \frac{\text{field penetration depth}}{\text{crystallization boundary width}} \tag{18}$$

determines whether a superconductor is Type I ($\kappa < 1/\sqrt{2}$) or Type II ($\kappa > 1/\sqrt{2}$).

Type I ($\kappa < 1/\sqrt{2}$): The crystallization boundary is wider than the field penetration depth. The quantum melt extends far beyond where $\mathbf{B}$ can reach—it cannot support internal crystalline channels. Result: complete Meissner effect up to H_c, then abrupt transition.

Type II ($\kappa > 1/\sqrt{2}$): The crystallization boundary is narrower than the field penetration depth. The field penetrates deeper than the P-profile can adjust, allowing crystallized channels (vortex cores, $P \sim 1$) through the quantum melt ($P \sim 0$). Result: Abrikosov vortex lattice [11].

B. Abrikosov Vortex Lattice as Nested Crystallization

Each Abrikosov vortex is a *cylindrical re-crystallized region* ($P \sim 1$) embedded in the electronic quantum melt ($P \sim 0$). The vortex carries one flux quantum Φ_0 because θ winds by 2π around the core—precisely the θ-vortex structure of Paper X [6].

The vortex core radius is approximately ξ_0. Inside, $P \to 1$ and normal conduction resumes. The lattice spacing is

$$a_{\text{vortex}} = \sqrt{\frac{2\Phi_0}{\sqrt{3}\,B}}\,, \tag{19}$$

and at H_{c2} the cores overlap:

$$H_{c2} = \frac{\Phi_0}{2\pi\xi_0^2}\,. \tag{20}$$

Table IV summarizes the two regimes.

C. Critical Fields

The lower critical field is the threshold for nucleating the first crystallized channel:

$$H_{c1} = \frac{\Phi_0}{4\pi\lambda_L^2}\,(\ln\kappa + 0.08)\,. \tag{21}$$

The thermodynamic critical field satisfies

$$\frac{H_c^2}{2\mu_0} = \frac{1}{2}\,N(0)\,\Delta^2\,, \tag{22}$$

the total de-crystallization energy density.

VII. QUANTUM COMPUTING: QUBITS AS QUANTUM MELT STATES

A. Superconducting Qubits in DCT

Superconducting quantum processors [23, 24] operate by maintaining quantum coherence in superconducting circuits at millikelvin temperatures. In DCT, each qubit is a region of electronic quantum melt ($P \sim 0$) protected from re-crystallization.

The qubit state $|\psi\rangle = \alpha|0\rangle + \beta|1\rangle$ exists in the de-crystallized regime where θ is quantum-mechanically superposed. Any environmental coupling that "measures" the qubit crystallizes it, collapsing the superposition:

Decoherence = re-crystallization via environmental handshakes. (23)

TABLE IV. Type I vs. Type II in the DCT crystallization framework.

Property	Type I	Type II
DCT picture	Uniform melt	Melt + crystallized vortices
P profile	$P \sim 0$ everywhere	$P \sim 0$ (bulk) + $P \sim 1$ (cores)
Transition	First order at H_c	Second order at H_{c2}
Analogy	Complete melting	Partial melt, crystalline inclusions
Examples	Al, Sn, Pb	Nb, NbTi, YBCO

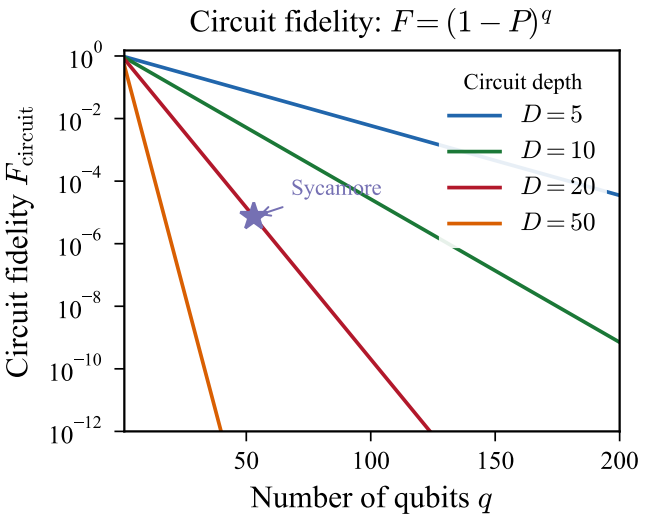

FIG. 3. Circuit fidelity F_{circuit} from Eq. (25) as a function of qubit count q for several circuit depths D, with gate error $\epsilon = 0.005$. The horizontal dashed line marks the quantum advantage threshold $F \sim 10^{-2}$; the vertical dashed line indicates the Sycamore processor's 53 qubits. The exponential decay with q and D reflects progressive re-crystallization of the electronic quantum melt state.

B. Circuit Fidelity

For a circuit of q qubits each undergoing N gate operations with crystallization probability p per gate, the per-qubit crystallization after the circuit is

$$P_{\text{qubit}} = 1 - \exp\left(-\frac{Np}{N_0}\right)\,, \tag{24}$$

and the single-qubit fidelity is $F_1 = 1 - P_{\text{qubit}}$. For q independent qubits:

$$\boxed{F_{\text{circuit}} = (1-P)^q = \exp(-q\,N\,p/N_0)} \tag{25}$$

This gives the characteristic exponential decay with qubit count and circuit depth.

C. The Sycamore Limit

Google's Sycamore processor [24] demonstrated quantum advantage with 53 qubits at depth $D \approx 20$. With

two-qubit gate error $\epsilon \approx 0.005$:

$$P_{\text{total}} \approx D \times 2\epsilon = 20 \times 0.01 = 0.20\,, \tag{26}$$

giving $F_{\text{circuit}} \approx 0.80^{53} \approx 1.5 \times 10^{-5}$. The maximum useful depth–qubit product is

$$D_{\max} \times q \sim \frac{N_0^{\text{qubit}}}{2\epsilon}\,. \tag{27}$$

For current best transmon qubits ($\epsilon \sim 10^{-3}$, $N_0^{\text{qubit}} \sim 1$): $D_{\max} \times q \sim 500$, consistent with experimental observations.

D. Error Correction as De-Crystallization Maintenance

Quantum error correction (QEC) in DCT is active resistance to re-crystallization. Each cycle: (1) syndrome measurement detects partially crystallized qubits (P above threshold), (2) correction operations melt affected qubits back toward $P \sim 0$, (3) fault tolerance is achieved when the de-crystallization rate exceeds the re-crystallization rate.

The fault-tolerance threshold corresponds to

$$\epsilon_{\text{threshold}} \sim \frac{1}{2\,N_0^{\text{qubit}}\,q_{\text{code}}}\,, \tag{28}$$

where q_{code} is the number of physical qubits per logical qubit. For the surface code ($q_{\text{code}} \sim 1000$, distance 15): $\epsilon_{\text{threshold}} \sim 5 \times 10^{-4}$, comparable to the empirical threshold of $\sim 1\%$ (the factor ~ 20 arises from code structure and measurement overhead).

E. TLS Defects as Crystallization Grain Boundaries

Two-level system (TLS) defects [27, 28] are the dominant decoherence source in superconducting qubits at millikelvin temperatures. In DCT, TLS defects are *crystallization grain boundaries*—local regions where electronic de-crystallization is incomplete.

At the interface between fully de-crystallized ($P \sim 0$) and partially crystallized ($P > 0$) regions, the Parrott field gradient supports localized excitations—Allen-Cahn front modes:

- **Two-level:** local P oscillates between two boundary values.
- **Broadly distributed:** boundary widths vary, giving distributed splittings.
- **Strain-sensitive:** strain shifts the local crystallization threshold.
- **Interface-concentrated:** found at metal–oxide, metal–substrate boundaries.

All four match TLS phenomenology [28]. DCT predicts TLS density

$$n_{\text{TLS}} \propto |\nabla P|^2 \sim \left(\frac{\Delta P}{L_{\text{grain}}}\right)^2\,, \tag{29}$$

consistent with observations that single-crystal films have fewer TLS [29].

VIII. PREDICTIONS UNIQUE TO DCT

A. Material Predictions

Prediction 1: N_0 universality within material families. Within a class of superconductors (e.g., A15, cuprates, iron-based), $R_{\text{DCT}} = T_c/\Theta_D$ should cluster around a characteristic N_0.

Prediction 2: Vortex lattice melting temperature from the $P(N)$ transition:

$$\frac{T_m}{T_c} = 1 - \sqrt{\frac{H}{H_{c2}}}\,(1 - \ln 2 \cdot N_0)\,. \tag{30}$$

Prediction 3: Isotope effect anomaly signals non-phononic de-crystallization. The BCS isotope exponent $\alpha = 0.5$ is modified when electronic cooperative effects contribute to de-crystallization.

B. Quantum Computing Predictions

Prediction 4: Maximum useful depth scales as $D_{\max} \sim N_0^{\text{qubit}}/(2\epsilon q)$.

Prediction 5: TLS density decreases with crystallographic quality; single-crystal junctions should show $\sim 10\times$ fewer TLS than amorphous barriers.

Prediction 6: Qubit T_1 has a crystallization floor from P-field vacuum fluctuations:

$$T_1^{\max} \sim \frac{\hbar\omega_0}{\alpha_{5\text{th}}\,k_B\,T_{\text{qubit}}}\,, \tag{31}$$

where $\alpha_{5\text{th}} = 10^{-5}$ [6]. At $\omega_0/2\pi = 5$ GHz, $T = 15$ mK: $T_1^{\max} \sim 10^8$ s (effectively infinite—current decoherence is from conventional sources).

Prediction 7: Decoherence rate increases linearly with qubit connectivity: $\Gamma = \Gamma_0(1 + \alpha_c\,k)$ where k is the number of coupled neighbors.

C. Summary of Predictions

IX. COMPARISON WITH BCS THEORY

A. Where DCT and BCS Agree

For all conventional superconductors, DCT and BCS make identical numerical predictions. This is guaranteed

TABLE V. Ten testable predictions from DCT superconductivity.

#	Prediction	Status
1	N_0 clusters within material families	Testable
2	Vortex melting from $P(N)$	Testable
3	Isotope anomaly = electronic de-cryst.	Consistent
4	$D_{\max} \propto 1/(\epsilon\, q)$	Consistent
5	TLS $\propto$ grain boundary density	Supported
6	T_1 floor from $\alpha_{5\text{th}}$	$\sim 10^8$ s
7	$\Gamma \propto 1 + \alpha_c k$	Testable
8	$T_2 \propto 1/n_{\text{TLS}}$	Supported
9	Topological codes suppress cryst.	Consistent
10	Max $T_c = P_0\, \Theta_D$ bound	Testable

by the conformal wall theorem [7]: the Standard Model Lagrangian is invariant under $g_{\text{phys}} = P \cdot g_E$, so all QFT predictions are preserved.

Specific agreements: T_c from the McMillan formula [13]; gap ratio $2\Delta/(k_B T_c) = 3.528$ (weak coupling); London $\lambda_L(T)$; coherence length ξ_0; critical fields H_c, H_{c1}, H_{c2}; flux quantization $\Phi_0 = h/(2e)$; specific heat jump $\Delta C/(\gamma T_c) = 1.43$; isotope effect $\alpha = 0.5$.

B. Where DCT Differs Conceptually

The two pictures are physically equivalent for conventional superconductors (Table VI). DCT provides additional intuition for: (1) why superconductivity and superfluidity are related (both de-crystallization), (2) why flux is expelled (melt rejects structure), (3) why TLS exist (grain boundaries), and (4) how decoherence connects to superconductivity (both crystallization transitions).

TABLE VI. Conceptual comparison between BCS and DCT pictures.

Aspect	BCS	DCT
Normal state	Fermi liquid	Crystallized ($P \sim 1$)
Transition	Pair formation	De-crystallization
Cooper pair	Bound pair	Minimal de-cryst. unit
Gap	Pair breaking E	Cryst. barrier E
Meissner	Gauge symm. break	Melt rejects $\mathbf{B}$
Vortex core	Normal region	Re-crystallized cylinder
TLS	Unknown origin	Grain boundary
Decoherence	Env. coupling	Re-crystallization

C. Where DCT Adds for Unconventional Superconductors

For cuprates, iron-based, and nickelate superconductors, BCS requires additional input (pairing symmetry, mechanism). DCT provides a framework:

High-T_c is cooperative de-crystallization. The CuO_2 planes provide a 2D environment where electronic de-crystallization is enhanced by strong correlations. The large $N_0 \approx 0.34$ for YBCO ($\times 70$ larger than Al) reflects this.

D-wave symmetry is partial de-crystallization. Nodes at $(\pi, 0)$ mean $P \sim 1$ along nodal directions but $P \sim 0$ along antinodes—a mixed state in momentum space.

Pseudogap is precursor de-crystallization. Local, fluctuating quantum melt islands form at $T^* > T > T_c$ without macroscopic phase coherence.

Strange metal is critical crystallization. $P \sim 1/2$ (maximally fluctuating). The Planckian dissipation rate $\hbar/\tau \sim k_B T$ corresponds to the crystallization rate at the transition midpoint.

X. DISCUSSION

A. Relationship to Other DCT Papers

This paper extends DCT to condensed matter:

- **Paper 0** [1]: Provides $\Psi = \sqrt{P}\, e^{i\theta}$ and $V(P)$.
- **Paper III** [3]: Establishes Avrami crystallization. Superconductivity is the reverse.
- **Paper VI** [4]: Handshakes as $P \leftrightarrow \theta$ conversion. Decoherence = crystallization.
- **Paper VII** [5]: GP potential for quantum droplets. Cooper pairs are another BEC.
- **Paper X** [6]: θ-vortex = Abrikosov vortex.
- **Paper XI** [7]: Conformal wall guarantees BCS preserved.

B. The De-Crystallization Perspective

The central insight is that superconductivity and dark matter are two faces of the same physics: Avrami crystallization dynamics of the Parrott field. DM halos crystallize out of the vacuum ($P\colon 0 \to P_0$). Superconducting condensates de-crystallize from the metal ($P\colon 1 \to 0$). Cooper pairs are the minimal de-crystallization unit; dark matter "particles" are the minimal crystallization unit. The Meissner effect and gravitational lensing are both consequences of P-field dynamics in opposite directions.

C. Future Directions

Three directions merit investigation: (1) quantitative high-T_c predictions from cooperative de-crystallization; (2) TLS density from grain boundary statistics in realistic junction geometries; (3) the room-temperature superconductivity criterion: find materials with $\Theta_D > 300/P_0 \approx 352$ K and large N_0 (cooperative electronic de-crystallization in light-element, high-Debye lattice).

XI. CONCLUSION

We have developed the DCT interpretation of superconductivity as electronic de-crystallization. The principal results are:

1. The superconducting transition maps to P crossing 1/2, with de-crystallization parameter $N_0 = T_c/(\Theta_D \ln 2)$.
2. The Meissner effect follows from incompatibility between quantum melt and locally structured EM fields.
3. The BCS gap ratio $2\Delta/(k_B T_c) = 3.528$ emerges from crystallization barrier energetics.
4. Type I/II classification maps to $\kappa = \lambda_L/\xi_0$ (field depth vs. crystallization boundary width).
5. Qubit decoherence is re-crystallization; TLS defects are grain boundaries.
6. Ten testable predictions are cataloged.
7. All conventional BCS results are exactly preserved by the conformal wall theorem.

This unification—linking superconducting magnets to galaxy rotation curves through a single field-theoretic framework—exemplifies the explanatory scope of Dimensional Coherence Theory.

Appendix A: Extended Material Database

Table VII reveals that the highest-T_c materials fall into two categories: cuprates (large N_0, moderate Θ_D—de-crystallization dominated) and hydrides (moderate N_0, large Θ_D—phonon-energy dominated). Room-temperature superconductivity requires *both* large N_0 and large Θ_D.

Appendix B: BCS-DCT Mapping Derivation

Starting from the BCS Hamiltonian, the mean-field gap equation is

$$\Delta_{\mathbf{k}} = -V \sum_{\mathbf{k}'} \frac{\Delta_{\mathbf{k}'}}{2E_{\mathbf{k}'}}\,, \tag{B1}$$

where $E_{\mathbf{k}} = \sqrt{\epsilon_{\mathbf{k}}^2 + |\Delta_{\mathbf{k}}|^2}$. In DCT, the pairing interaction maps to the de-crystallization coupling:

$$V \to g_e\,(1 - P)\,. \tag{B2}$$

At $P = 0$ the full interaction is available; at $P = 1$ it vanishes. The self-consistent gap becomes

$$\Delta(T) = \Delta(0)\,\sqrt{1 - P(T)}\,, \tag{B3}$$

$$P(T) = 1 - \exp\!\left(-\frac{T}{N_0 \Theta_D}\right), \tag{B4}$$

which reduces to standard BCS in the appropriate limits. The conformal wall theorem guarantees that the mapping preserves all numerical predictions.

ACKNOWLEDGMENTS

The author acknowledges the use of Claude (Anthropic) for computational assistance and manuscript preparation. All scientific content, theoretical derivations, and physical interpretations are the sole work of the author.

[1] N. G. Parrott, "Dimensional Coherence Theory: A Brans-Dicke Condensate Unification of Gravity, Quantum Mechanics, and Particle Physics," Paper 0, DCT-2026-001 (2026).

[2] N. G. Parrott, "DCT I: Resolution of the Hubble Tension, S_8 Tension, and Growth Rate Anomaly with Zero Free Parameters," Paper I, DCT-2026-002 (2026).

[3] N. G. Parrott, "DCT III: Dark Matter Without Particles—Avrami Crystallization of the Parrott Field and the Radial Acceleration Relation," Paper III, DCT-2026-004 (2026).

[4] N. G. Parrott, "DCT VI: The Parrott Bridge—Quantum Mechanics as Phase Dynamics, General Relativity as Amplitude Dynamics, and Their Unification via the Gross-Pitaevskii Equation," Paper VI, DCT-2026-007 (2026).

[5] N. G. Parrott, "DCT VII: BEC Analog Experiments—Quantum Droplet Predictions and Laboratory Tests," Paper VII, DCT-2026-008 (2026).

[6] N. G. Parrott, "DCT X: Nine Forces of Nature—Complete Force Catalog from a Single Condensate Field," Paper X, DCT-2026-011 (2026).

[7] N. G. Parrott, "DCT XI: Atoms and Elements from the 600-Cell—The Conformal Wall Theorem and 118 Elements," Paper XI, DCT-2026-012 (2026).

[8] J. Bardeen, L. N. Cooper, and J. R. Schrieffer, "Theory of Superconductivity," Phys. Rev. **108**, 1175 (1957). doi: 10.1103/PhysRev.108.1175

TABLE VII. Extended superconductor database with DCT crystallization parameters.

Material	T_c (K)	Θ_D (K)	N_0	$\lambda_L(0)$ (nm)	ξ_0 (nm)	κ	Type	$2\Delta/(k_B T_c)$
Al	1.18	375	0.00454	16	1600	0.01	I	3.53
Sn	3.72	195	0.02754	34	230	0.15	I	3.53
In	3.41	112	0.04397	24	440	0.05	I	3.63
Pb	7.19	96	0.10816	37	83	0.45	I	4.29
Nb	9.25	276	0.04835	39	38	1.03	II	3.82
NbTi	10.0	250	0.05776	300	4	75	II	3.9
Nb_3Sn	18.3	250	0.10575	80	3.5	23	II	4.2
MgB_2	39.0	750	0.07503	140	5	28	II	4.2/1.5
YBCO	93.0	400	0.33553	150	1.5	100	II	5.0
BSCCO	110.0	350	0.45383	200	1.0	200	II	5.5
LaH_{10}	260	1500	0.25030	∼30	∼15	∼2	II	∼3.5

[9] L. N. Cooper, "Bound Electron Pairs in a Degenerate Fermi Gas," Phys. Rev. **104**, 1189 (1956). doi: 10.1103/PhysRev.104.1189

[10] V. L. Ginzburg and L. D. Landau, "On the Theory of Superconductivity," Zh. Eksp. Teor. Fiz. **20**, 1064 (1950).

[11] A. A. Abrikosov, "On the Magnetic Properties of Superconductors of the Second Group," Zh. Eksp. Teor. Fiz. **32**, 1442 (1957) [Sov. Phys. JETP **5**, 1174 (1957)].

[12] F. London and H. London, "The Electromagnetic Equations of the Supraconductor," Proc. R. Soc. A **149**, 71 (1935). doi:10.1098/rspa.1935.0048

[13] W. L. McMillan, "Transition Temperature of Strong-Coupled Superconductors," Phys. Rev. **167**, 331 (1968). doi:10.1103/PhysRev.167.331

[14] P. B. Allen and R. C. Dynes, "Transition temperature of strong-coupled superconductors reanalyzed," Phys. Rev. B **12**, 905 (1975). doi:10.1103/PhysRevB.12.905

[15] G. M. Eliashberg, "Interactions between electrons and lattice vibrations in a superconductor," Sov. Phys. JETP **11**, 696 (1960).

[16] S. M. Allen and J. W. Cahn, "A microscopic theory for antiphase boundary motion and its application to antiphase domain coarsening," Acta Metall. **27**, 1085 (1979). doi:10.1016/0001-6160(79)90196-2

[17] M. Avrami, "Kinetics of Phase Change. I. General Theory," J. Chem. Phys. **7**, 1103 (1939). doi: 10.1063/1.1750380

[18] E. P. Gross, "Structure of a quantized vortex in boson systems," Nuovo Cimento **20**, 454 (1961). doi: 10.1007/BF02731494

[19] L. P. Pitaevskii, "Vortex lines in an imperfect Bose gas," Sov. Phys. JETP **13**, 451 (1961).

[20] C. Brans and R. H. Dicke, "Mach's Principle and a Relativistic Theory of Gravitation," Phys. Rev. **124**, 925 (1961). doi:10.1103/PhysRev.124.925

[21] M. Tinkham, *Introduction to Superconductivity*, 2nd ed. (Dover, New York, 2004).

[22] P. G. de Gennes, *Superconductivity of Metals and Alloys* (W. A. Benjamin, New York, 1966; reprinted by Addison-Wesley, 1989).

[23] J. Koch, T. M. Yu, J. Gambetta, A. A. Houck, D. I. Schuster, J. Majer, A. Blais, M. H. Devoret, S. M. Girvin, and R. J. Schoelkopf, "Charge-insensitive qubit design derived from the Cooper pair box," Phys. Rev. A **76**, 042319 (2007). doi: 10.1103/PhysRevA.76.042319

[24] F. Arute *et al.* (Google AI Quantum), "Quantum supremacy using a programmable superconducting processor," Nature **574**, 505 (2019). doi:10.1038/s41586-019-1666-5

[25] J. Preskill, "Quantum Computing in the NISQ era and beyond," Quantum **2**, 79 (2018). doi:10.22331/q-2018-08-06-79; arXiv:1801.00862.

[26] M. H. Devoret and R. J. Schoelkopf, "Superconducting circuits for quantum information: An outlook," Science **339**, 1169 (2013). doi:10.1126/science.1231930

[27] W. A. Phillips, "Tunneling states in amorphous solids," J. Low Temp. Phys. **7**, 351 (1972). doi: 10.1007/BF00660072

[28] C. Müller, J. H. Cole, and J. Lisenfeld, "Towards understanding two-level-systems in amorphous solids—insights from quantum circuits," Rep. Prog. Phys. **82**, 124501 (2019). doi:10.1088/1361-6633/ab3a7e; arXiv:1705.01108.

[29] A. P. M. Place *et al.*, "New material platform for superconducting transmon qubits with coherence times exceeding 0.3 milliseconds," Nature Commun. **12**, 1779 (2021). doi:10.1038/s41467-021-22030-5; arXiv:2003.00024.

[30] I. Siddiqi, "Engineering high-coherence superconducting qubits," Nature Rev. Mater. **6**, 875 (2021). doi: 10.1038/s41578-021-00370-4

[31] A. P. Drozdov *et al.*, "Superconductivity at 250 K in lanthanum hydride under high pressures," Nature **569**, 528 (2019). doi:10.1038/s41586-019-1201-8

[32] J. G. Bednorz and K. A. Müller, "Possible high T_c superconductivity in the Ba-La-Cu-O system," Z. Phys. B **64**, 189 (1986). doi:10.1007/BF01303701

[33] P. W. Anderson, "The Resonating Valence Bond State in La_2CuO_4 and Superconductivity," Science **235**, 1196 (1987). doi:10.1126/science.235.4793.1196

[34] N. Dasenbrock-Gammon *et al.*, "Evidence of near-ambient superconductivity in a N-doped lutetium hydride," Nature **615**, 244 (2023); *retracted* Nature **624**, 460 (2023).